Clay Mineral Analysis in the Appalachian Valley-and-Ridge Province: Implications for depositional environment, temperature conditions and folding

Lindsey Abdale
University of Michigan
Honors Thesis April 2017

ABSTRACT

Mineralogical trends of grain size fractions from 27 samples taken from the Appalachian Valley and Ridge province in the eastern US provide information on depositional environment, temperature conditions of formation, and mechanisms of folding. Samples were disaggregated into five clay-sized fractions through centrifugation and analyzed with an X-Ray diffractometer (XRD) to determine qualitative mineralogy. Samples were then matched with standards of IM_d and $2M_1$ Illite polytypes to determine proportion of authigenic to detrital material, respectively. Results show all samples to contain illite, chlorite and quartz, and with high concentrations (90%) of authigenic illite in the finest (<0.05 μm) grain sizes. The mineralogical trends, including iron oxides or evaporates, are associated with depositional environments of eight formations: the Reedsville formation, Juniata formation, Bald Eagle formation, Bloomsburg formation, Rose Hill Formation, McKenzie formation, Wills Creek formation, and Marcellus (and equivalent formations). The abundance of secondary, low friction clay minerals provide an explanation for widespread, flexural slip folding that occurred in the area.

INTRODUCTION

This study examines mineralogical trends associated with grain size fractions of shale and clay rich rock samples from the Valley and Ridge Province of the Central Appalachian Mountains to determine depositional environment, temperature conditions of formation and mechanisms of folding. Previous studies have identified generalized mineralogy and depositional environments of the major formations within the Appalachian Mountain belt and basin and their deformation; for example, Miller and Erikkson (2000) used outcrop stratigraphy and Sak (2012) used map and strain data to create a balanced geologic cross section of the region. The current study provides detailed mineralogy of the formations from XRD analysis of 27 samples to determine sediment source origin, post-deposition temperature conditions and resulting alteration of sampled shales. Temperature conditions of formation for the samples in this study is constrained by ubiquitous presence of chlorite as a secondary replacement feature of the IIb polytype that forms at low temperatures, below 200°C, in carbonates, as explained by Moore and Reynolds (1997). Studies such as Tembe et al. (2010) and Morrow et al. (1992) have shown that illite and chlorite minerals have low sliding resistance (coefficient of friction). The presence of low coefficients of friction minerals in these sample shale beds promotes flexural slip folding that would explain the abundance of narrow hinged folds and kink-band folding observed in the Valley and Ridge Province (see also Hodge, 2013).

Understanding the mineralogy of these samples is important for several reasons including: (1) the black shales of our samples are associated with oil formation (Cooper, 2007), (2) understanding the depositional environment will asses presence of ore deposits at a regional scale (Perazzo, 1968; Smith, 1995), (3) samples' relative proportion of authigenic material can be radiometrically dated to source the age, from 100% detrital illite (Fitz-Diaz, 2014) (4) authigenic clay from burial diagenesis may explain the widespread presence of flexural slip folds that are related to more deeply buried thrust faults (Hodge, 2013).

Cooper (2007) performed a statistical analysis of reserves in fold-thrust belts indicates these settings are the most prolific in hydrocarbons. Particularly, most of the reserves are in thin-skinned fold-thrust belts that have no salt seal and that are partially buried by sediments, as occurs in the Appalachian Valley and Ridge province. Studies by Barrett (2008) show how the Marcellus black shale in the region exemplifies natural gas traps in low-permeability shales, and studies in Perazzo (1968) review mineral resources mined in the Valley and Ridge province including limestone, zinc and iron. Studies linking mineralogical trends and depositional environments presented in this paper provide a structural and sedimentological understanding for societal resources.

This study also provides the required work to date deformation using radiometric $^{40}Ar/^{39}Ar$ dating techniques. Once dated, samples are organized based on radiometric ages of (five) clay-size fractions against the illite composition and extrapolated to 0% detrital illite (=100% authigenic illite) to determine the age of authigenic illite, and thus the timing of deformation, as discussed in Fitz-Diaz (2014) and earlier studies. This paper utilizes past studies on the coefficients of friction for clay minerals to examine the kinematics of flexural slip within the major fold structures of the Appalachian Valley and Ridge Province. Haines and van der Pluijm (2012), Tembe et al. (2010) and Moore and Lockner (2004) assess the role of clay minerals similar to those found in our samples (illite and chlorite), which have relatively low coefficients of friction compared to most rock forming minerals. According to experiments outlined in Hodge (2013), thin beds of weak shales would be expected to produce narrow hinged folds and kink-bands. Mineralogical studies of clays presented in this paper support the regional abundance of kink-band folding in the valley and Ridge Province of Appalachian Mountain belt.

This thesis presents a systematic mineralogical study by high-resolution XRD techniques to determine depositional environment, conditions of formation, as well implications for folding by examining and cataloging the range of clay occurrences that are found in the Appalachian Valley and Ridge Province. The methods in this study rely on modern XRD theory and analysis to understand crystal structure, as first outlined in Moore and Reynolds (1997) as well as properties of clay minerals as originally outlined in Brindley and Brown (1980) in order to asses conditions of formation and related structural kinematics.

BACKGROUND

Tectonic History

The Appalachian Mountains extend 3,000 km, trending southwest on the eastern coast of the United States. The mountain belt formed during a complete Wilson cycle involving three orogenic events which followed on an earlier history that began with the Grenville orogeny in the late Mesoproterozoic.

Early tectonics: Beginning in the Late Mesoproterozoic, the Grenville orogeny assembled several continental masses into the supercontinent Rodinia, which now appears as basement rocks of the continental margin (Faill, 1997; Hibbard, 2003). Continuing from the Late Neoproterozoic to the Early Cambrian, the eastern margin of supercontinent Laurentia

developed extensional rifting as the plate pulled away from Gondwana, forming the Iapetus ocean. Following extension, siliciclastic sediments were deposited on the eastern margin of Laurentia during the Late Cambrian. Two microcontinents were positioned to the east of Laurentia in this sea. To the east of the microcontinents, magmatic arcs developed during the convergence within the Iapetus ocean and were thrust over microcontinents during collision (Faill, 1997).

Taconic orogeny: In the Middle to Late Ordovician the microcontinents and magmatic arcs continued to converge westward, and were eventually thrust on top of Laurentia from the east (Faill, 1997). This Taconian suture consisted of major fault and terrane boundaries with mafic and ultramafic rocks from the magmatic arcs including detrital zircons that confirm their distal origin (Hatcher, 2010).

Acadian orogeny: Following a steady carbonate shelf throughout the Paleozoic, the Acadian orogeny formed as a result of the zippering north to south closing of the Iapetus ocean as the Peri-Gondwanan superterranes collided with Laurentia, as seen in Fig. 2, producing polyphase deformation and high-grade metamorphism (Hatcher, 2010).

Alleghany Orogeny: Beginning in the North-Central Appalachians in the Early Permian, as seen in Fig. 2, (Faill, 1997), this event was caused by the convergence and collision between supercontinents Laurentia and west Gondwana. Decollement tectonism, a deformational structure of basal detachment involving a gliding plane between two rock masses (van der Pluijm, 2004), occurred in eastern Laurentia, now the central and southern Appalachians. Very low angle thrust decollement originated at mid-crustal levels east of the present Appalachians and rose westward. Deformation developed in the hanging-wall block (the allochthon) through thrust faults and fold-thrust structures that splayed upward from the basal detachment.

The youngest products of the Alleghany orogeny are observed in the northeast trending strike-slip faults and dextral shear zones in the Piedmont region, see Fig. 1. In the northern-central Appalachians, the exposed allochthon includes a sedimentological region (the Appalachian Plateau and Valley and Ridge Province) and a crystalline region (the Blue Ridge Mountain belt and Piedmont Province), as seen in Fig. 1. The sedimentological region is dominated by long anticlines and include widespread layer-parallel shortening that preceded the folding, while the crystalline region is dominated by east northeast trending low angle thrust faults and folds (Faill, 1997).

Valley and Ridge Province

The structures of the Valley and Ridge are a result of shortening and thickening events associated with the collision of supercontinents Gondwana and Laurentia in the Late Carboniferous Alleghany orogeny (Hatcher, 2010, Sak, 2012). From the Late Carboniferous to Early Jurassic, Gondwana was rotated into further collision with southeastern Laurentia, producing the Blue Ridge Piedmont megathrust sheet, as seen in Fig. 1 (Faill, 1997; Hatcher, 2010). Following this orogenic event, the Piedmont ridge and other parts of the Appalachians were eroded and sediments were fed in large amounts to offshore basins during the Mesozoic to the Cenozoic. The mountain belt has been dormant ever since.

In present day, the structure of the valley and ridge province can be categorized into three main features. The basement consists of Neoproterozoic crystalline and sedimentary rocks. Overlying this is a faulted sequence of Cambrian to Ordovician carbonates. The surface consists of a folded cover sequence of Ordovician to Pennsylvanian foreland basin siliciclastic rocks as seen in purple in Fig. 3 overlying a thrust detachment as marked in red in Fig. 3 (Sak, 2012). The fold thrust belt was separated from the carbonate shelf rocks by this decollement and above we find imbricate thrusts that coalesce into a roof thrust within the Reedsville formation (Gwinn, 1964, 1970; Rodgers, 1963, 1970; Sak 2012).

CLAY MINERALS

Structure and properties

Clay minerals are hydrous aluminum silicates classified as phyllosilicates, or sheet silicates (Moore and Reynolds, 1997). Most have well-developed (001) cleavage (Moore and Reynolds, 1997) that gives the thin sheet appearance that is characteristic in hand specimen. All sheet silicates have patterns of alternating layers of corner-linked tetrahedra (T) and edge-linked octahedra (O) sheets; kaolinite is called a 1:1 layer silicate structure because it has alternating tetrahedra octahedra layers (TO/TO), illite is a 2:1 layer silicate because it has two tetrahedra for every one octahedra sheet forming octahedra sandwiches (TOT/TOT), and chlorite is considered a 2:1:1 layer silicate because it has an extra octahedra layer within the 2:1 pattern (TOT/O/TOT/O) (Moore and Reynolds, 1997). Disorder may cause rotations or translations between layers and if these displacements are systematic, polytypes are generated, as seen in Fig. 7 (Brindley, 1980; Moore and Reynolds, 1997).

Clay minerals have charged surfaces that define their ion-exchange capacities, dispersion/flocculation behavior, transport and fate of solutes, rates of chemical weathering and erodibility (Moore and Reynolds, 1997). There are two kinds of surface charges: one comes from cation substitution with one less valence charge which often leads to single ions or ionic groups in between layers to restore neutrality, the other exists at edges of particles at the ends of broken bonds where the chemical composition or structure may only be maintained with additional ions (usually H^+ or OH^-) to satisfy the bonds (Moore and Reynolds, 1997). This produces a variable charge which is a function of the pH of the surrounding medium (Moore and Reynolds, 1997). Cations are attracted to the (001) surface whereas anions attach to the edges. Clays may also contain an electric double layer which occurs when particles are able to approach each other closely and van der Waals forces bind the particles into clumps, otherwise referred to as flocculation (Moore and Reynolds, 1997).

Illite

Compositionally, illite is an end member series phyllosilicate between muscovite and smectite (Moore and Reynolds, 1997). Illite has more Si, Mg and H_2O, but less tetrahedral Al and less interlayer K than muscovite. Basal reflections for illite have a *d*(001) of 10 Å and are

identified by a peak at 8.8° 2θ (Moore and Reynolds, 1997). The $1M_d$ - $2M_1$ sequence reflects increasing temperature and pressure conditions (Moore and Reynolds, 1997). The appearance of the $2M_1$ polytype coincides with the beginning of the lowest temperature (sub-200°C) metamorphic zone (Weaver and Brockstra, 1984). Once all illite $2M_1$ a new zone of the high-temperature smectite to illite transition begins, which represents the transformation of illite into mica (Moore and Reynolds, 1997). Illites can express the environment in which they formed because those found in shales and those found in sandstones vary according to the permeability and available space to grow (Moore and Reynolds, 1997).

X-RAY DIFFRACTION THEORY

X-Ray Diffractometer

X-Ray diffraction techniques are fundamental for crystal structure analysis and are especially useful for clay minerals that are <2 μm and, therefore, too small for other optical or scanning electron microscopy (Moore and Reynolds, 1997). Electromagnetic radiation propagates along straight lines at 300,000 km per second in a vacuum, it also reflects and refracts according to Snell's law and diffracts at edges, slits or gratings (Klein, 2007). When electrons moving at high velocities strike any material, X-rays are produced. In an X-ray diffractometer, electrons are generated within the X-Ray tube and bombard a target material to produce continuous and characteristic X-ray spectra. X-ray tubes are vacuums with a tungsten filament serving as cathode that provides the source of electrons (Klein, 2007). The X-ray diffractometer used in this study has a Copper (Cu) anode. To emit electrons, the filament is heated through a passage of current and a high voltage applied across the tube accelerates the emitted electrons towards the target anode. X-rays are generated when the electrons hit the anode and are emitted in all directions. When the X-rays strike the crystal structures in our oriented powder slides, the electrons in the collision path vibrate with the same frequency as the incident X-radiation (Fig. 5). These electrons absorb and scatter some of the energy from the X-ray and the scattered waves interfere in certain directions where waves are inphase and diffraction occurs, according to Bragg's law (Klein, 2007).

Bragg's Law

W.L. Bragg showed how diffraction takes place from a set of parallel crystal planes if conditions satisfy the Bragg's law equation $n\lambda = 2d\sin\theta$, where n is an integer, λ *i*s a given wavelength, d is the distance between parallel planes, and θ is the angle of incidence and reflection of the X-ray beam from the plane as illustrated in Fig. 6 (Klein, 2007). 2θ is obtained from the XRD record, and one can use Bragg's law to determine the d spacing of the crystal lattice (Brindley and Brown,1980.)

METHODOLOGY

Sampling Methods

In order to determine the mineralogy of the Valley and Ridge Province, shale samples in the foreland fold-thrust belt of the US Central Appalachians were collected along four transects across central Pennsylvania, eastern Maryland and eastern West Virginia (Fig. 8). We sampled from several major fold structures in thrust sheets at exposures along US-22 W and US-322 W between State College and Harrisburg, PA, as well as US-522 W and US-22 W to the south of that between Cumberland and Hagerstown, MD. At each outcrop, samples were collected from shale and clay rich units in visible meso faults and folds after digging into the exposure to avoid effects of surface weathering. 42 samples were taken from eight major formations: the Middle Ordovician Reedsville formation, the Late Ordovician Juniata formation, the Late Ordovician Bald Eagle formation the Early Silurian Bloomsburg formation, the Middle Silurian Rose Hill formation, the Middle Silurian McKenzie formation, the Late Silurian Wills Creek formation, and the Early Devonian Marcellus (and equivalent formations).

Sample preparation

Samples were first washed with deionized water to remove any visible organic material or salts. Samples were then disaggregated by hand using an agate mortar and pestle, suspended in deionized water, and placed in a Branson 3510 ultrasonic bath for ~5 minutes to promote further separation of clay-sized grains. According to Stoke's Law, samples were then spun in a Thermo Scientific CL-2 centrifuge for 1 min and 20 sec at 1,000 rpm to separate bulk clay sizes of <2 μm. Suspended <2 μm fractions were poured into a vessel to air dry slowly. Once dry, the separated size fraction was manually scraped out, re-suspended in deionized water, and separated into a <0.05 μm size fraction for 59.38 mins at 5000 rpm. This process, with varying RPM's and running times, was continued to separate a total of six clay size fractions (<2 μm for bulk, <0.05 μm for fine, 0.05-0.1 μm for medium-fine, 0.1-0.5 μm for medium, 0.5-1 μm for medium-coarse and 1-2 μm for coarse.)

Oriented clay mounts were then prepared for XRD characterization. ~300 mg of bulk size fractions were suspended in ~5 mL deionized water and placed on glass slides using a dropper according to the suspension method as discussed in Moore and Reynolds (1997), then left to air dry in an oven at 50° C.

Dried sample slides were exposed to glycol for at least 8 hours at 50°- 60°C to increase vapour pressure of the glycol. Mixed layer clays often contain both swelling and non-swelling layers (Brindley and Brown, 1980). Ethylene glycol saturation standardizes swelling so that XRD results can be examined for integral or non-integral spacings to recognize smectite or not.

X-ray Analysis

XRD characterization of clay-sized fractions was used to determine the presence of illite and to characterize the detailed mineralogy. Each slide was scanned from 2°-30° 2θ using a

copper source Rigaku Ultima IV XRD at an accelerating voltage of 40 kV and filament current of 44 mA at a speed of 1° per minute with a nickel-foil Kβ filter installed. Sheet silicates lie flat in oriented slides which intensifies XRD peaks for expandible sheet silicates and makes their characteristic peaks more easily identifiable. Intensity peak profiles of our samples can be compared to published mineral reference intensities of various clays (Reynolds 1997) using the computer program MacDiff.

Polytype Quantification

After qualitative mineralogy, modern computer techniques were used to quantify clay polytype proportions from X-ray spectra. From previous studies (e.g., Reynolds 1963; Haines 2008; Fitz-Diaz, 2014) we know that that illite in fault gouge and folds contains a mixture of detrital clays derived from the wall rock, and authigenic clays that formed during faulting and folding in the brittle upper crust (Fitz-Diaz, 2014). Shallow crustal faulting at low temperatures prevents the syntectonic mineral recrystallization seen in deeper faults. Thus, both old detrital and newly grown authigenic fine-grained phyllosilicates are preserved (van der Pluijm, 2008). The age of the wall rock and the age of detrital components reflect the age of regional cooling, when original sediments were formed and deposited, while authigenic components reflect the age when alteration, diagenesis and faulting occurred. These previous works have also determined that, in a grain fraction of illite <2 μm, the $1M/1M_d$ polytype reflects low-temperature authigenic growth, whereas the $2M_1$ polytype represents the detrital, host rock component.

Polytypes of clay minerals refers to silicate sheets with varying stacking sequences as seen in Fig. 7 (Moore and Reynolds 1977; Haines 2008). We distinguish between $1M_d$ and $2M_1$ polytypes through XRD pattern analysis by scanning random powder mounts along with $2M_1$ and $1M_d$ mineral standards under the same conditions and machine parameters. We match end members through the method outlined in Haines (2008) to determine the proportion of illite polytypes between size fractions in each sample. Standard XRD patterns for the $1M_d$ and $2M_1$ end members are input into a spreadsheet and proportionately mixed to match the patterns of the samples with a +/-2-3% error, as seen in Fig. 10.

RESULTS

Mineralogical Trends

XRD analyses from oriented samples reveals each sample to contain multiple clay mineral phases, most commonly illite and chlorite. The mineralogy of samples is summarized in Table 1. Qualitative observations of these data show a general trend of decreasing concentrations of chlorite and smectite with decreasing grain size, as seen in Fig 10.

Other non-clay mineral phases are also present in the samples. Quartz is present in every sample with higher amounts in the coarse fractions and lower amounts in the fine size fractions. Feldspar is observed in 17 samples and, similarly to quartz, shows decreasing concentrations with decreasing grain size. Calcite is observed in 7 samples and shows varying trends in relation to grain size between samples. Evaporates such as gypsum are also seen in

six samples but do not follow any observable trend associated with grain size. Trace amounts of iron oxides can be observed in three samples (MD WC 13, PA RH 37, MD WC 42) but do not appear with high enough concentrations to show any trends associated with grain size.

Clay Mineral Quantification

The results from the end-member standard matching quantification methods described earlier are summarized in Table 2, which include calculated total proportions of authigenic ($1M_d$) relative to detrital ($2M_1$) illite. For all samples, the relative proportion of authigenic illite increased with decreasing grain size, as is commonly observed in prior studies(eg. Fitz Diaz, 2014). Most samples contain high proportions (>90%) of detrital illite in the fine size fractions, such as sample in Fig 10., whereas (MD WC 12 and PA WC 25 show lower (70%) detrital in their fine size fractions.)

DISCUSSION

Mineralogy and Depositional Environment

The samples were obtained and analyzed from eight major formations, and the sample mineralogy reflects the depositional environment and conditions of their respective formations.

- Reedsville formation: This formation consists of Middle Ordovician shale with a distal turbidite sequence deposited on a carbonate shelf during the Taconic orogeny that deformed the Reedsville formation at very low metamorphic grade (Wright, 1985). The detrital illite, chlorite and quartz in the Reedsville samples likely came from the original turbidite sequence, with trace amounts of calcite originating on the carbonate shelf or precipitating later as cement.
- Juniata formation: This Late Ordovician formation is defined with grey-red-green thin interbedded siltstone and shale units and very fine to medium grained cross-bedded sandstones with interbedded conglomerates. The depositional environment is mostly terrestrial to shallow marine produced during the Taconic Orogeny (Darton, 1896; Berg, 1980). Our shale sample from this formation contained quartz and trace amounts of feldspar which assumably originated from the original terrestrial deposition.
- Bald Eagle formation: This formation is also Late Ordovician and reflects the same depositional environment as well as sample mineralogy as the Juniata formation above (Darton, 1896; Berg, 1980).
- Bloomsburg formation: This formation is made up of red claystone, argillaceous siltstone, red shale and very fine sandstone in fining upwards cycles. Sediments in this formation include terrestrial and shallow marine, which accumulated in the foreland basin during the Taconic orogeny (Berg, 1961). The red color and presence of iron phosphates and iron oxides in our samples from this formation reflect the post-depositional oxidizing conditions.

- Rose Hill formation: This Middle Silurian formation was deposited under fluvial to shallow marine conditions (Smosna, 1978). Our samples from this formation likely originated in fluvial environments because no calcite was observed.
- McKenzie formation: Also Middle Silurian in age, the McKenzie interbedded limestone, sandstone and shale represents a subaerial to shallow-subtidal condition limited to a shelf setting (Smosna, 1978). The shallow marine shelf setting is well represented in our samples through carbonates such as calcite and evaporates such as gypsum.
- Wills Creek formation: This formation represents thin bedded mudstone, calcareous shale, argillaceous limestone and sandstone ~420 Ma in age and forms the bedrock for most of Pennsylvania (Smosna, 1978). This formation developed as uninterrupted deposition in the Appalachian Basin and surrounding mudflats (Smosna, 1978). All of our samples from this formation contained calcite which reflects the limestone lithology.
- Marcellus formation and equivalent Devonian shales: This formation developed during the Acadian orogeny as eroded continental sediments that were deposited seaward through deltaic systems in relatively deep and anoxic environments (Barrett, 2008). Our samples from this formation contain quartz and trace feldspar from the continental lithics as well as clays and trace calcite from the sea environment.

Mineralogy and clay formation conditions

The presence of chlorite is ubiquitous in the samples. Chlorite ideally consists of a negatively charged 2:1 layer with a positively charged octahedral sheet (Moore and Reynolds, 1997). The most common cation substitutions include Mg^{2+}, Fe^{2+}, Al and Fe^{3+}(Moore and Reynolds, 1997). Chlorites are most commonly found in shales at highest grades of diagenesis, in soils, on surface of sand grains within porous sandstones as an alteration product, as a replacement of carbonate grains and matrix in carbonate rocks or in geothermal and low temperature hydrothermal systems (Moore and Reynolds, 1997). Shale and limestone samples contain chlorite as a replacement of carbonate grains. Most chlorites in shales and slates are the IIb polytype which can form at low temperatures (below 200°C) without passing through any intermediate polytypes (Walker, 1987, 1993). The chlorite crystallization in cavities of our carbonate samples signify a low temperature formation across all samples and formations (Walker, 1987).

Feldspar appears in decreasing concentrations with decreasing grain size in 14 of our samples. These mineral grains are detrital and distinctly not authigenic. There are no feldspars present in the fine grained fraction, indicated both that there was no fine grained feldspars to begin with, and that our methods of disaggregation did not significantly alter grain size(Moore and Reynolds, 1997).

Quartz abundance decreases with decreasing grain size indicating quartz as a primary lithology from continental erosion as opposed to a secondary cementation which would have grown from the smallest grain sizes. We would expect the opposite trend if secondary quartz had grown interstitially in our samples.

Calcite followed a decreasing abundance trend with decreasing grain size in WV DS 9, MD BF 14 and MD WC 42 suggesting calcite as a primary feature. MD McK 4 and MD MS 1

showed calcite in the fine fraction suggestion calcite grew as a secondary precipitate in these samples. Larger grains likely had a longer time to grow, whereas finer grains indicate the mineral had limited space and time to grow.

Iron oxides found in clay size fractions in samples MD WC 13, PA RH 37 and MD WC 42 as a function of depositional environment just like the detrital illite.

Evaporates, most commonly gypsum, did not follow any trends associated with grain size and their presence can therefore be considered a primary feature as a function of the depositional environment of the formation.

Frictional Properties and Flexural Slip Folding

The presence illite and chlorite clay minerals from several major fold structures in thrust sheets reflect a low frictional strength that promotes flexural slip among layers. Illite and chlorite have relatively low coefficients of friction (represented by the symbol μ) compared with most rock-forming minerals, m=0.65-0.80 (Haines and van der Pluijm, 2012). Illite has a reported frictional strength of μ=0.50 to 0.60 for dry conditions (Haines and van der Pluijm, 2012) and μ=0.27-0.32 for saturated conditions at 10-60 Mpa (Tembe et al., 2010; Haines and van der Pluijm, 2012). Chlorite strength values range from μ=0.6 in dry conditions (Morrow et al., 1992; Haines and van der Pluijm, 2012) and 0.27 to 0.38 for saturated conditions (Moore and Lockner, 2004; Haines and van der Pluijm, 2012). The widespread occurrence of minerals with these low coefficients of friction facilitated the flexural slip mechanism of folding, and explains the abundance of narrow hinges and mesoscale kink-band folding. According to Hodge (2013), freely-slipping, thin-layered mediums such as the sampled shale layers, should lead to kink-like forelimbs and backlimbs with flat fold crests, as is observed in the field and seen in Fig. 9.

CONCLUSION

Composition of rock samples and mineralogical trends from grain size analysis in folds in the Valley and Ridge Province of the Central Appalachians reflect the depositional and low-temperature alteration conditions of eight formations. Mineralogic analysis shows that samples contain high abundances of the clay minerals illite and chlorite, and non-clay minerals, most commonly quartz, carbonates, evaporates, iron oxides and trace feldspar. Importantly, they have high (up to 90%) authigenic illite in the finest grain sizes reflecting regional alteration at low temperatures. The abundance of low coefficients of friction clay minerals provide an explanation for flexural slip folding that is found along the major structures on the area. Understanding the conditions of clay mineralization is also important because the sampled shales are associated with economic deposits, including oil, gas and coal and, therefore, the mineralization conditions represent those of economic deposits. Thirdly, the formation of authigenic material can be radiometrically dated using ratios of detrital and authigenic clays as determined in this study, which is the target of future work. The presence of clay minerals govern the mechanics of folding and brittle faulting in the area, resulting in widespread occurrence of flexural slip folds.

Acknowledgements

I would like to thank Erin Lynch for her mentorship in field work, laboratory methods, theory and paper editing. I am grateful to Ben van der Pluijm for the research opportunity and academic guidance. NSF partially supported my research. I also thank Zhongrui Li at the University of Michigan Electron Microbeam Analysis Laboratory (EMAL) for assistance with X-ray diffraction.

References

Barrett, R., 2008, The Depositional Setting of the Marcellus Black Shale (PDF): Appalachian Producers Issues Seimnar, Independent Oil and Gas Association of West Virginia.

Berg, T.M., Edmunds, W.E., Geyer, A.R., et al., 1980, Geologic Map of Pennsylvania and adjacent states: G36: Pennsylvania Geologic Survey, Harrisburg, Pennsylvania, scale 1:250,000.

Bove, D., Elber, D., McCarty, D., Meeker, G., 2002, Characterization and modeling of illite crystal particles and growth mechanisms in a zoned hydrothermal environment, Lake City, Colorado: American Mineralogist, v. 87, p. 1546-1556.

Cooper, M., 2007, Structural style and hydrocarbon prospectivity in fold and thrust belts: a global review: Geological Society of London, special publication, v. 272, p. 447-472.

Darton, N.H., and Taff, J.A., 1896, Description of the Piedmont sheet (West Virginia-Maryland): U.S. Geological Survey Geologic Atlas of the United States, Piedmont folio, no. 28, p. 6.

Davis, D., Suppe, J., and Dahlen, F.A., 1983, Mechanics of foldand-thrust belts and accretionary wedges: Journal of Geophysical Research, v. 88, p. 1153–1172.

Faill, R.T., 1997, Geologic History of the North-Central Appalachians: American Journal of Science, v. 297, p. 551-619.

Fitz-Diaz, 2014, Progressive, episodic deformation in the Mexican Fold-Thrust Belt (central Mexico): evidence from isotopic dating of folds and faults: International Geology Review, doi: 10.1080/00206814.2014.896228.

Gwinn, V.E., 1964, Thin-skinned tectonics in the Plateau and northwestern Valley and Ridge provinces of the central Appalachians: Geological Society of America Bulletin, v. 75, p. 863-900, doi: 10.1130/0016-7606(1964)75[863:TTITPA]2.0.C0;2.

Haines, S., 2008, Transformations in clay-rich fault rocks: Constraining fault zone processes and the kinematic evolution of regions: Dissertation.

Hatcher, R.D., 2010, The Appalachian orogen: A brief summary: Geological Society of America Memoirs, v. 206, p. 1-19,
doi: 10.1130/2010.1206(01)

Hodge, A.M., 2013, Influence of flexural slip on the form of fault related folds: Indiana University, Bloomington. Department of Geological Sciences, Masters Abstracts International, v. 51-06, p. 45.

Hibbard, J.P., 2003, The Appalachian Orogen - An Essay by James Hibbard: (can't find the publisher)

Hnat, J.S., van der Pluijm, B.A., 2014, Fault gouge dating in the Southern Appalachians, USA: Geological Society of America Bulletin, v. 126, is. 5-6, p. 639-651.

Klein C., Dutrow, D., 2007, Manual of Mineral Science: Wiley Publishing, ed. 23.

Miller, D.J., Eriksson, K.A., 2000, Sequence Stratigraphy of Upper Mississippian Strata in the Central Appalachians: A record of Glacioeustasy and Tectoneustasy in a Foreland Basin Setting: The American Association of Petroleum Geologists, v. 84, p. 210-233, doi: 10.1306/C9EBCDAB-1735-11D7-8645000102C1865D

Moore, D.M., Reynolds, R.C., 1997, X-Ray Diffraction and the Identification and Analysis of Clay Minerals: New York, Oxford University Press, p. 364.

Moore, D., Lockner, D., 2004, Crystallographic controls on the frictional behavior of dry and water-saturated sheet structure minerals: Journal of Geophysical Research B, doi: 10.1029/2003JB002582.

Morrow, C., Radney, B., Byerlee, J., 1992, Frictional strength and the effective pressure law of montmorillonite and illite clays *in* Evans, B., Wong, T.F. (Eds.), Fault Mechanics and Transport Properties of Rocks, p. 69-88.

Perazzo, P.B., Perazzo, P.G., 1968, Mineral Resources of the Appalachian Region *in* Stone Quarries and Beyond: http://quariesandbeyond.org (accessed April 2017).

Ramsay, B., 2008, The Depositional Setting of the Marcellus Black Shale (PDF): Appalachian Producers Issues Seminar, Independent Oil and Gas Association of West Virginia.

Rodgers, J., 1963, Mechanics of Appalachian foreland folding in Pennsylvania and West Virginia: American Association of Petroleum Geologists Bulletin, v. 47, p. 1527-1536.

Rodgers, J., 1970, The tectonics of the Appalachians: New York, Wiley-Interscience, p. 271.

Sak, P.B., McQuarrie, N., Oliver, B.P., Lavdovsky, N., Jackson, M.S., 2012, Unraveling the central Appalachian fold-thrust belt, Pennsylvania: The power of sequentially restored balanced cross sections for a blind fold-thrust belt: Geosphere.

Sattarzadeh, Y., Cosgrove, J.W., and Vita-Finzi, C., 2000, The interplay of faulting and folding during the evolution of the Zagros deformation belt, *in* Cosgrove, J.W. and Ameen, M.S., eds., Forced folds and fractures: Geological Society of London Special Publication 169, p. 187-196, doi: 10.1144/GSL.SP.2000.169.01.14.

Scotese, C.R., 2003, PALEOMAP Project: http://www.scotese.com (accessed March 2017).

Smith, R.C., 1995, Lead and Zinc in Central Pennsylvania: Pennsylvania Geological Survey.

Smosna, R., Patchen, D., 1978, Silurian evolution of central Appalachian Basin: AAPG Bulletin, v. 62, is. 11, p. 2308.

Tembe, S., Locknar, D., Wont, T.F., 2010, Effect of clay content and mineralogy on frictional sliding behavior of simulated gouges: binary and ternary mixtures of quartz, illite, and montmorillonite: Journal of Geophysical Research B 115, doi: 10.1029/2009JB006383.

van der Pluijm, B.A., 2004, Earth Structure: New York, NY: W.W. Norton, p. 457.

Walker, J.R., 1987, Structural and Compositional Aspects of Low-Grade Metamorphic Chlorite: Ph.E. Dissertation, Dartmouth College, Hanover, N.H.

Walker, J.R., 1993, Chlorite poltype geothermometry: Clays and Clay Minerals, v. 41, p. 260-267.

Weber, J., 2009, Appalachian map: U.S. Geological Survey, 1 sheet.

Weaver, C.E., Brockstra, B.R., 1984, Illite-mica *in* Weaver, C.E., and associates, Shale Slate Metamorphism in the Southern Appalachians: Elsevier, Amsterdam, p. 67-199.

Wright, T.O., 1985, Structures in the Fort Loudon, Pennsylvania locality of the Ordovician Reedsville formation: Journal of Structural Geology, v. 7, is. 3, p. 501, doi: 10.1016/0191-8141(85)90107-5

FIGURES

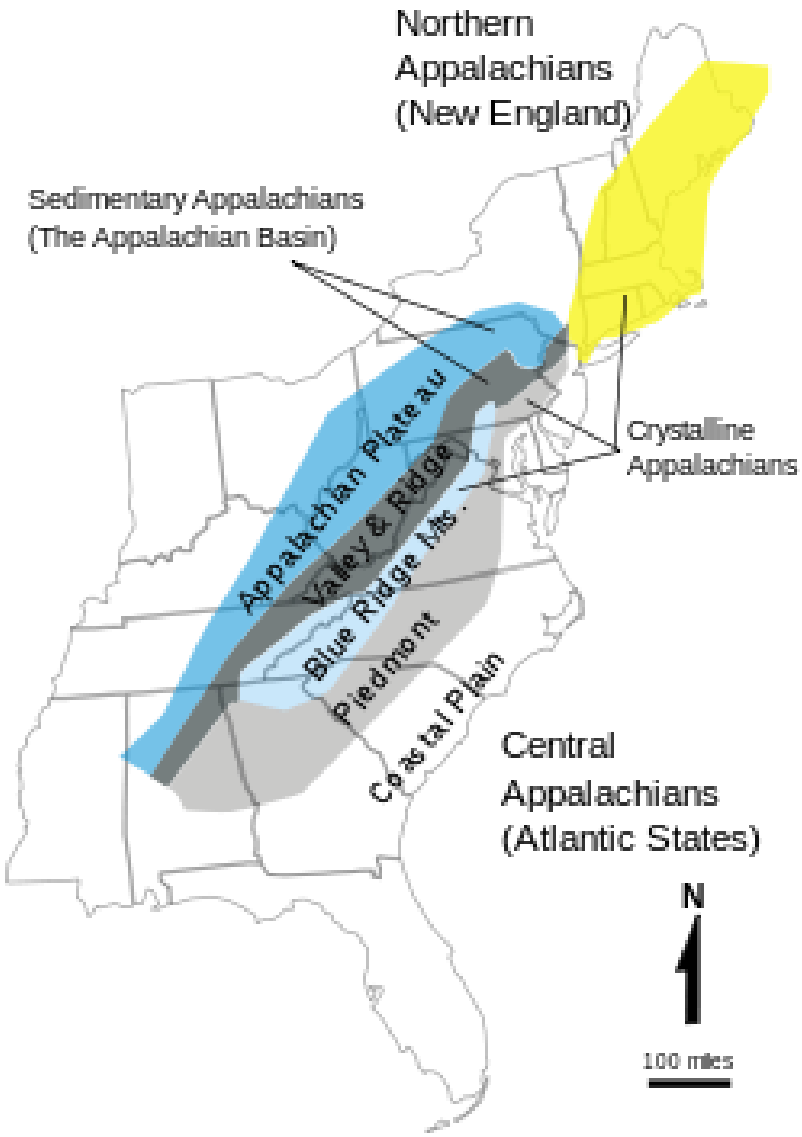

Figure 1. Map of the Appalachian Mountains region showing the structural belts of the "Sedimentary Appalachians" (dominated by anticlines and underlain by Paleozoic sedimentary rocks) and the "Crystalline Appalachians" (dominated by low-angle thrust faults and folds and underlain chiefly by Precambrian and Early Paleozoic metamorphic and igneous rocks) (Weber, 2009).

A

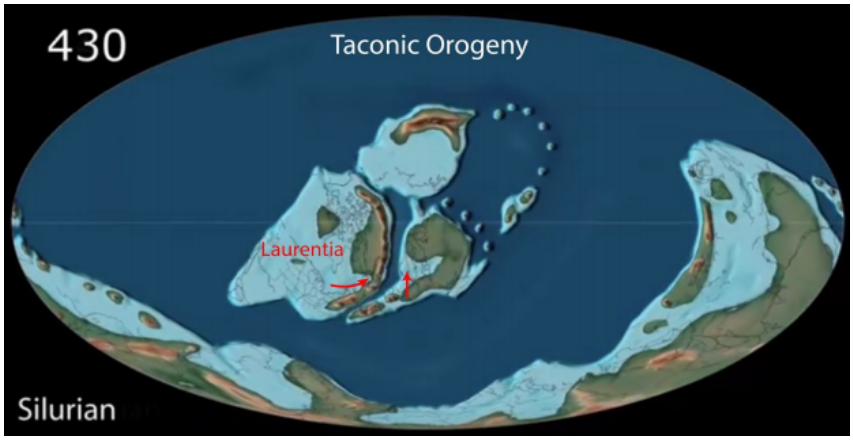

B

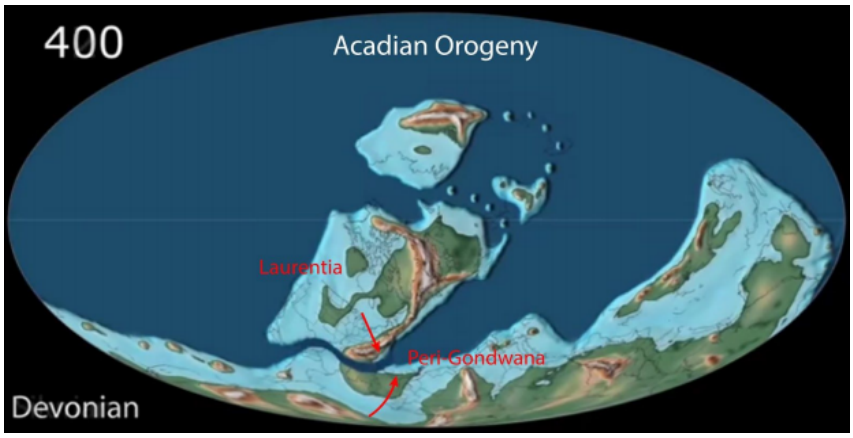

C

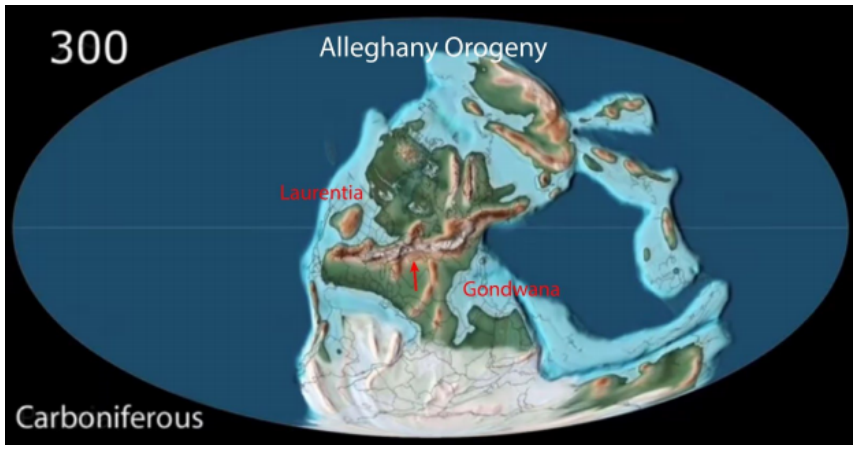

Figure 2. Maps showing plate movement involved in Taconic, Acadian and Alleghany Orogenies. Time are steps shown in upper left corner (in Ma), geologic Periods are indicated lower left corner, orogeny title is located in the upper center and supercontinent titles including relative plate motion indicated in red (Scotese, 2003). Map A indicates Silurian Taconic Orogeny collision of microcontinents and magmatic arcs with Laurentia. Map B shows Devonian Acadian Orogeny involving the closing of the Theic ocean and the collision of Laurentia and Peri-Gonwanan superterranes. Map C illustrates the Carboniferous Alleghany Orogeny including the convergence of Laurentia and Gondwana.

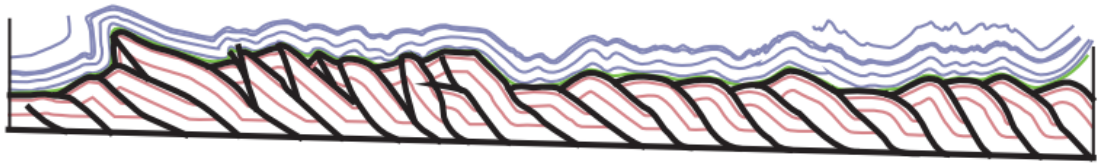

Figure 3. Simplified cross section of surface rock from the southern boundary of the Valley and Ridge province to the Appalachian Plateau. The red formation illustrates the passive thrust detachment structure dominated by Cambrian and Lower Ordovician Carbonates. The Purple illustrates the folded cover sequence of Ordovician to Pennsylvanian foreland basin siliciclastic rocks (Sak, 2012).

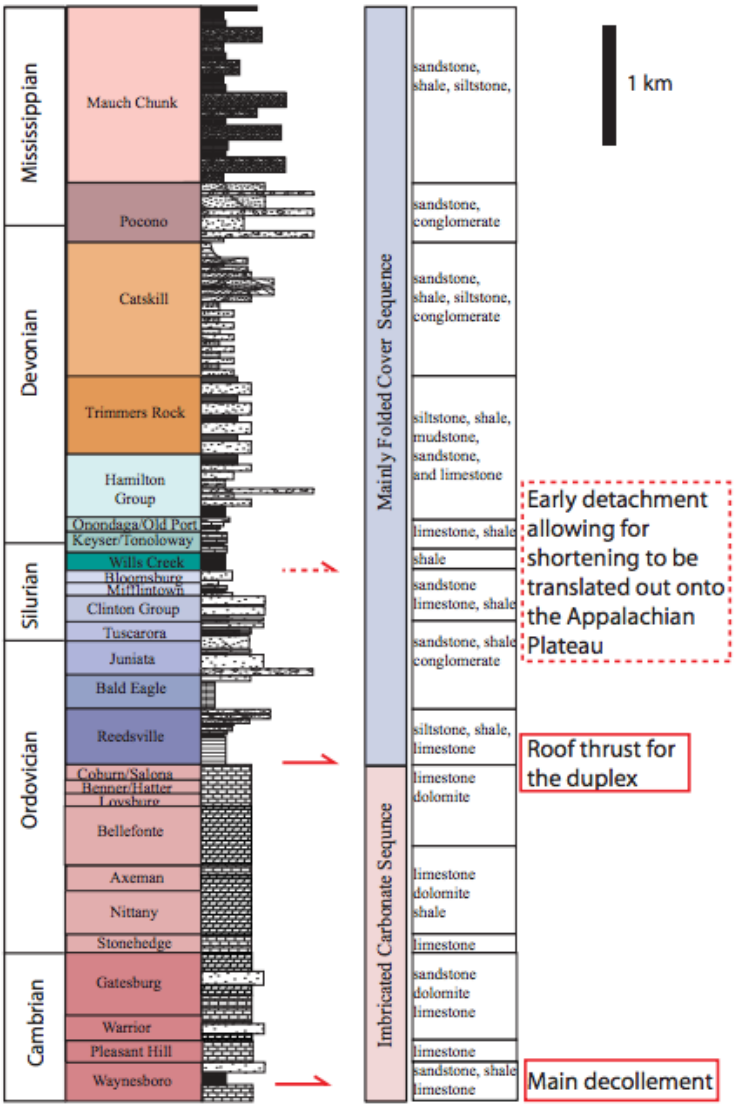

Figure 4. Stratigraphic column for the central Appalachian Valley and Ridge Province compiled by Sak (2012.) Column indicates date and formation of the main decollement as well as the roof thrust (indicated with red arrows). Our study sampled between the Reedsville and Devonian Marcellus.

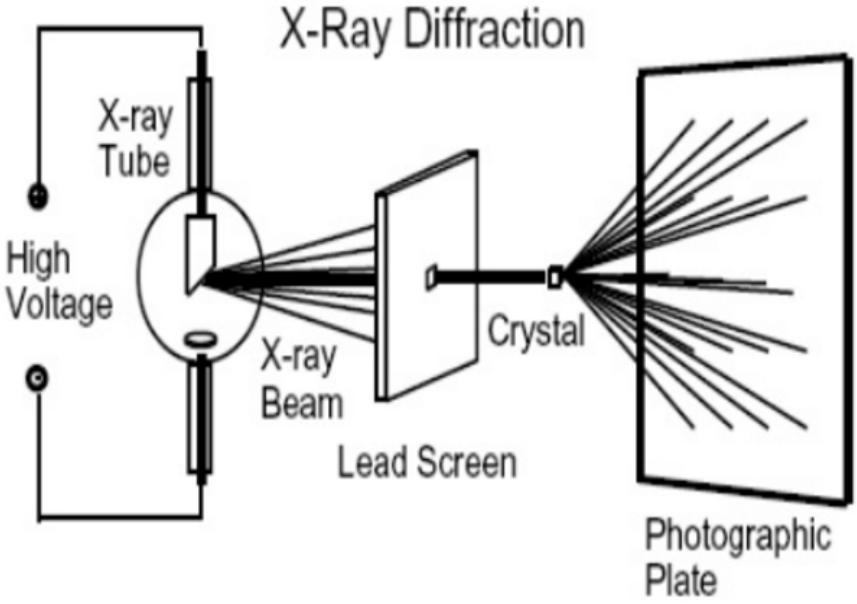

.

Figure 5. A schematic representation of X-ray diffraction. The high voltage electrical current heats the tungsten filament within the vacuum X-ray tube, causing electrons to be emitted. The differential voltage between the filament and the target metal accelerates the electrons toward the target. Once electrons hit the target, the X-ray beam is produced and directed towards the crystal through the lead screen (Klein, 2007).

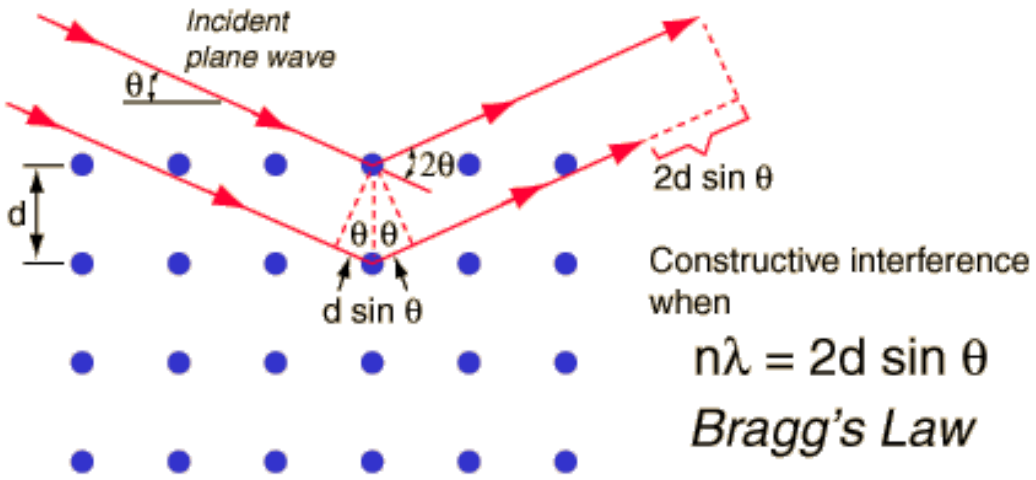

Figure 6. Conditions for X-ray diffraction from a row of atoms. When X-rays are diffracted from a crystal lattice, peaks of scattered intensity are observed when the angle of incidence and the angle of scattering are the same, as well as when the pathlength difference is an integer number of wavelengths, *n*. *λ i*s a given wavelength, *d* is the distance between parallel planes, and θ is the angle of incidence and reflection of the X-ray beam from the plane (Klein, 2007).

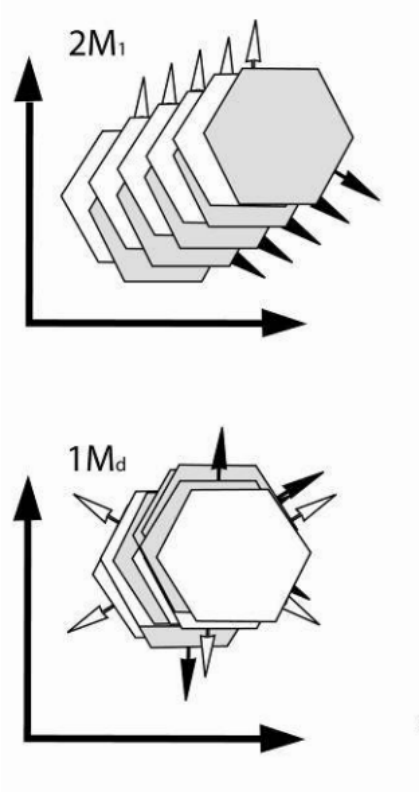

Fig 7. Illustrating translation and rotation between layers of $2M_1$ and IM_d illite polytypes (Haines, 2008).

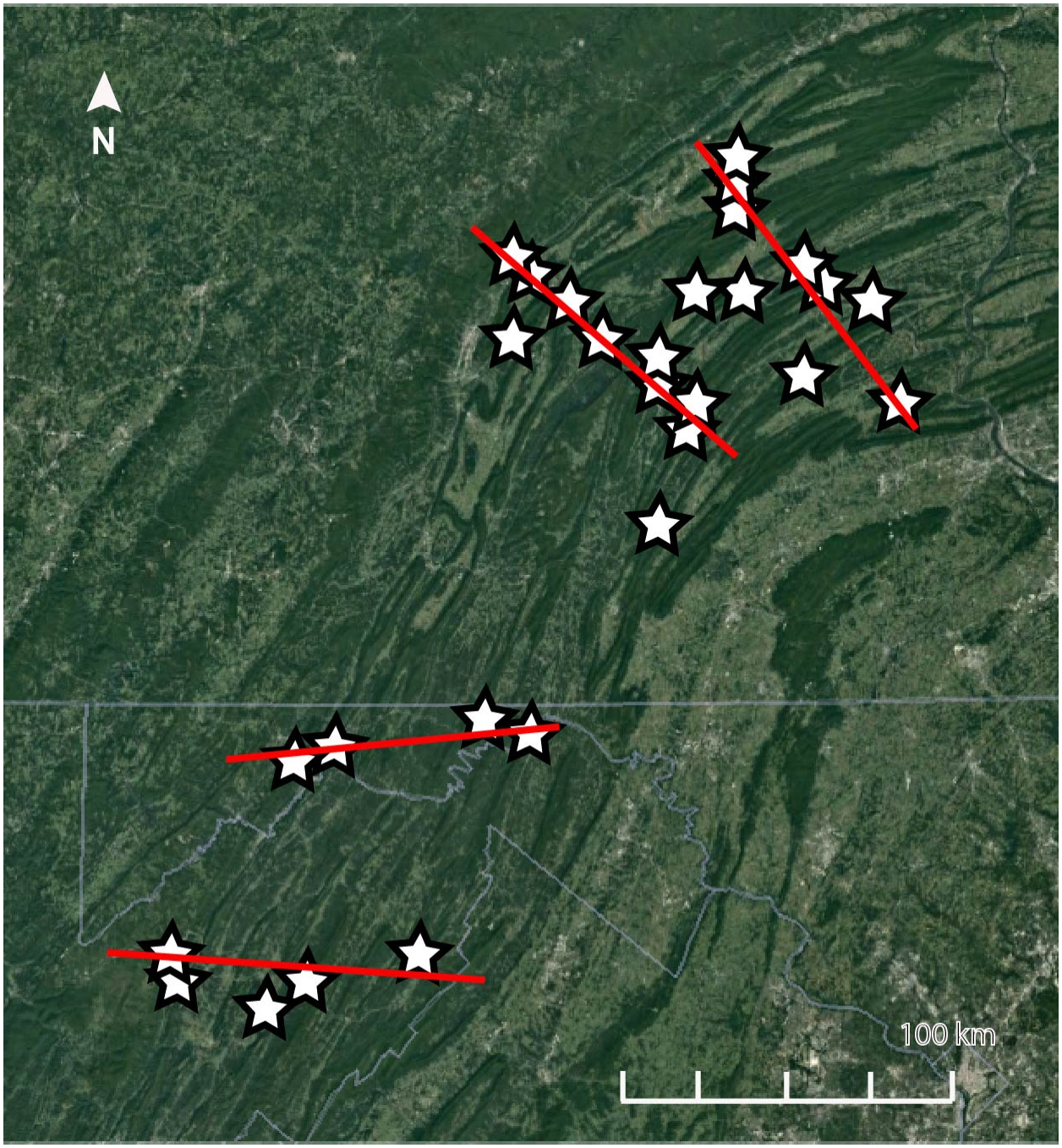

Figure 8. Map showing sample locations (starred) and transects (red lines).

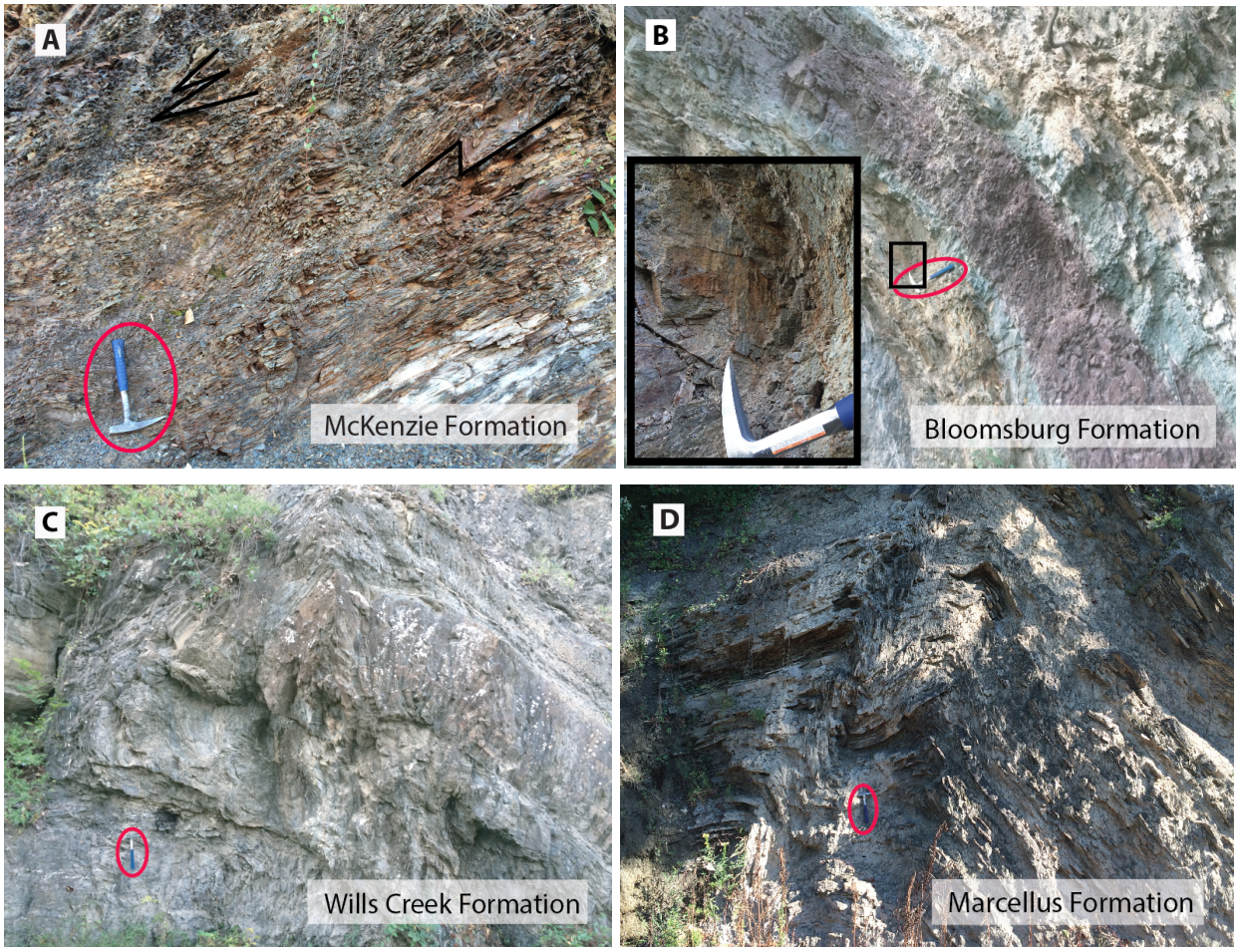

Figure 9. Field photographs of sample outcrops: (A) Taken from east limb of Wills Mountain (lat long), showing kink band folding, (B) Sampled along flexural slip surface showing slickenlines, (C) Shows mesoscale thrust and associated fold, (D) Taken along sheared sheared shales of mesoscale anticline. Note rock hammer for scale, indicated by red oval.

A. Oriented Slides

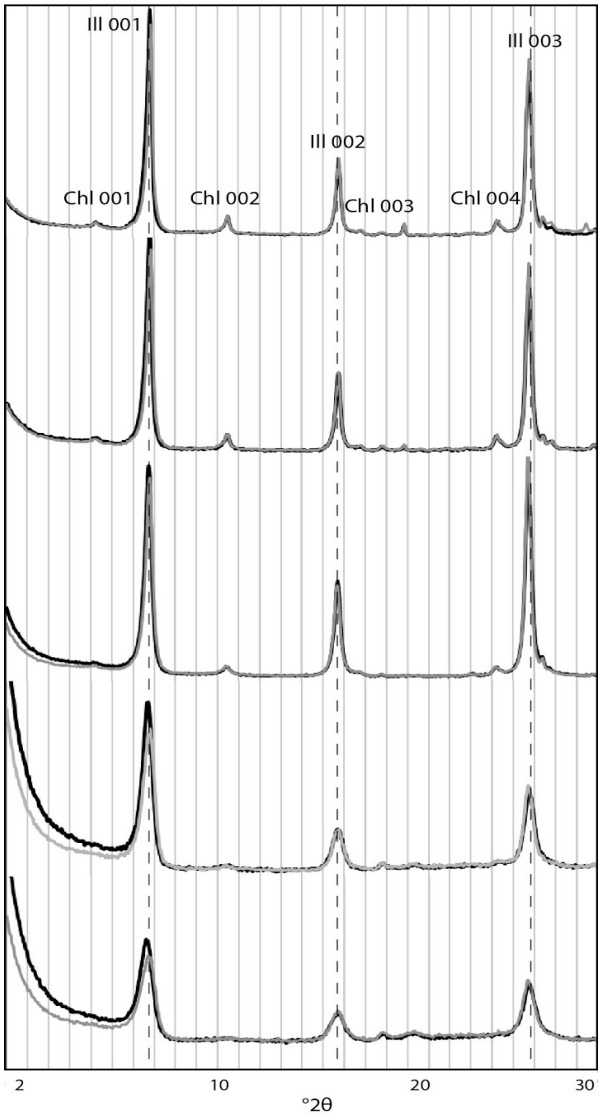

B. Random Powder Mounts

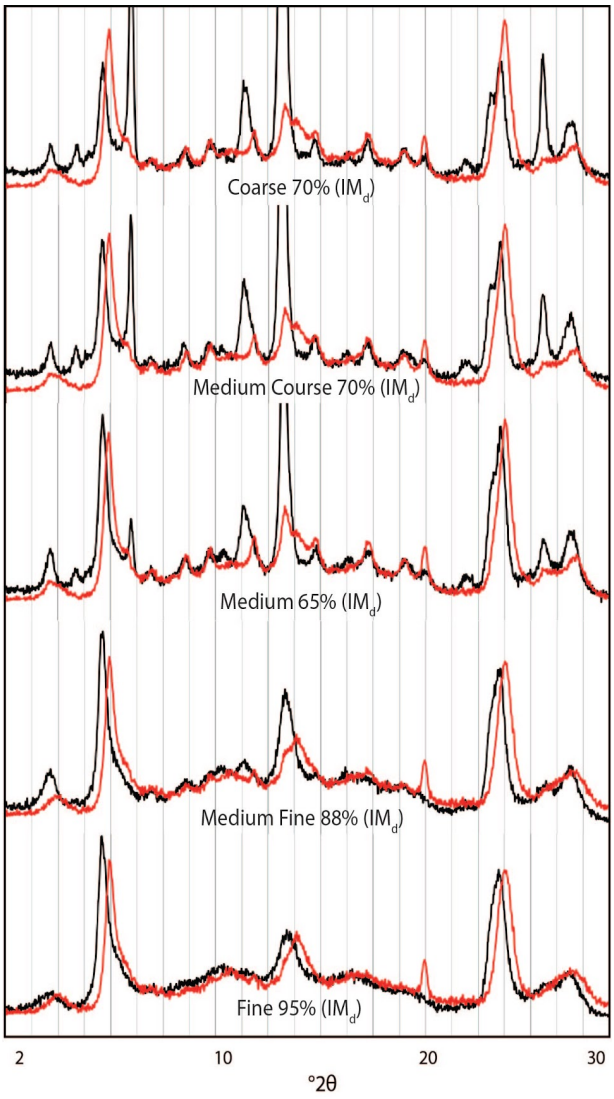

C. Polytype Standards

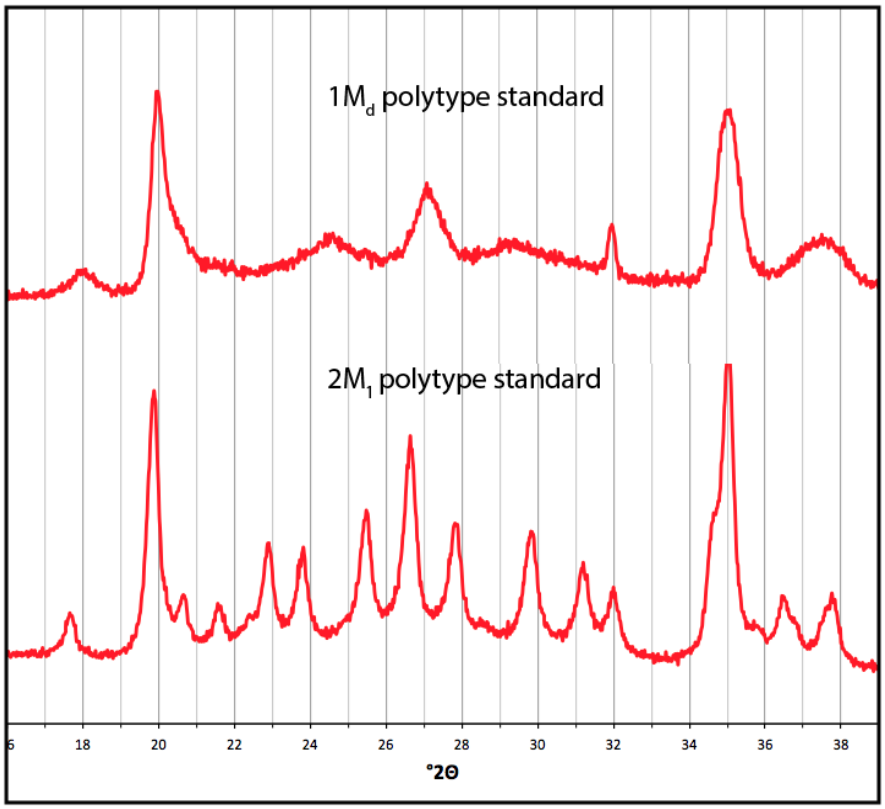

Figure 10. Representative XRD patterns used for analysis of composition and clay polytype. The patterns show five size fraction from a single sample, MD BF 14, with coarse at the top and fine at the bottom of each column. (A) Oriented slide XRD patterns show a trend of decreasing chlorite in progressively finer fractions. (B) Standards matching results from randomly oriented powder mounts. The XRD patterns are shown in black, while the modeled patterns are shown in grey. (C) Shows patterns for scanned IM$_d$ and 2M$_1$ polytype standards used to match with samples.

TABLES

Table 1

Sample	Illite	Chlorite	Quartz	Calcite	Feldspar	Gypsum	Fe Oxides
MD BF 14 C	x	x	x	x	x		
MD BF 14 MC	x	x	x	x			
MD BF 14 M	x	x	x				
MD BF 14 MF	x	x	x	x			
MD BF 14 F	x						
MD McK 16 C	x	x	x				
MD McK 16 MC	x	x	x				
MD McK 16 M	x	x			x		
MD McK 16 MF	x						
MD McK 16 F	x						
MD McK 4 C	x	x	x				
MD McK 4 MC	x	x	x				
MD McK 4 M	x	x	trace				

MD McK 4 MF	x	x				
MD McK 4 F	x			x		
MD MS 1 C	x	x	x		trace	
MD MS 1 MC	x	x	x			
MD MS 1 M	x	x			x	
MD MS 1 MF	x	x		trace		
MD MS 1 F	x	x				
MD WC 12 C	x	x	x			
MD WC 12 MC	x	x	x			
MD WC 12 M	x	x	trace			
MD WC 12 MF	x	trace				
MD WC 12 F	x					
MD WC 13 C	x	x	x			x
MD WC 13 MC	x	x	x	x		x
MD WC 13 M	x	x	trace			x
MD WC 13 MF	x	trace				

MD WC 13 F	x					x	
MD WC 42 C	x	x	x	trace			x
MD WC 42 MC	x	x	x	x			
MD WC 42 M	x	x		trace			
MD WC 42 MF	x	trace					
MD WC 42 F	x			x			
PA DS 19 C	x		x				
PA DS 19 MC	x	x	x				
PA DS 19 M	x	trace					
PA DS 19 MF	x	trace					
PA DS 19 F	x				x		
PA DS 24 C	x	x	x				
PA DS 24 MC	x	x	x				
PA DS 24 M	x	x	x		x		
PA DS 24 MF	x	x			trace		
PA DS 24 F							

PA F 28 C	x	x	x			
PA F 28 MC	x	x	x	x		
PA F 28 M	x	x	trace			
PA F 28 MF	x	x				
PA F 28 F	x	trace				
PA JF 32 C	x	x	x			
PA JF 32 MC	x	x	x			
PA JF 32 M	x	x	x			
PA JF 32 MF	x	x		trace		
PA JF 32 F	x	trace				
PA RH 37 C	x	x	x			x
PA RH 37 MC	x	x	x			
PA RH 37 M	x	x	trace			
PA RH 37 MF	x	x				
PA RH 37 F	x	x		trace?		
PA RS 26 C	x	x		x		

PA RS 26 MC	x	x	trace	trace
PA RS 26 M	x	x		x
PA RS 26 MF	x	x		x
PA RS 26 F	x			
PA RS 35 C	x	x	x	x
PA RS 35 MC	x	x	x	x
PA RS 35 M	x	x	x	x
PA RS 35 MF	x	x		
PA RS 35 F	x	trace		trace
PA RSBE 31 C	x	x	x	
PA RSBE 31 MC	x	x	x	x
PA RSBE 31 M	x	x	x	
PA RSBE 31 MF	x	x		
PA RSBE 31 F	x	x		
PA S 18 C	x	x	x	x
PA S 18 MC	x	x	x	x

PA S 18 M	x	x	x	trace?	x	
PA S 18 MF	x	x				
PA S 18 F	x	x			x	
PA SS 40 C	x		x			
PA SS 40 MC	x		x			
PA SS 40 M	x		x		x	
PA SS 40 MF	x					
PA SS 40 F	x					
PA WC 25 C	x	x	x			
PA WC 25 MC	x	x	x			x
PA WC 25 C						
PA WC 25 MF	x	x				x
PA WC 25 F	x					
WV DM 10 C	x	x	x			
WV DM 10 MC	x	x	x			
WV DM 10 M	x	trace				

WV DM 10 MF	x	x			
WV DM 10 F	x				
WV DS 9 C	x	x	x		
WV DS 9 MC	x	x	x	x	
WV DS 9 M	x	x	x	x	
WV DS 9 MF	x	x			
WV DS 9 F	x	x			
WV McK 7a C	x	x	x		
WV McK 7a MC	x	x	x		
WV McK 7a M	x	x	trace		
WV McK 7a MF	x	trace			
WV McK 7a M	x				
WV OS 6 C	x	x	x		x
WV OS 6 MC	x	x	x		x
WV OS 6 M	x	x	trace		x
WV OS 6 MF	x	x			

WV OS 6 F	x				
MD BF 14 ADO	x	x			
MD BF 14 EG C	x	x	x		
MD BF 14 ADO MC	x	x			x
MD BF 14 EG MC	x	x			
MD BF 14 ADO M	x	x			
MF BF 14 EG M	x	x			
MD BF 14 ADO MF	x				
MD BF 14 EG MF	x				
MD BF 14 ADO F	x				
MD BF 14 EG F	x				

Table 2

Sample	Size Fraction	%1M
MD-MS-1	coarse	50
	med-coarse	58
	medium	68
	medium-fine	83
	fine	90
MD-RH-3	coarse	60
	med-coarse	65
	medium	76
	medium-fine	92
	fine	93
MD-McK-4	coarse	40
	med-coarse	45
	medium	50
	medium-fine	85
	fine	88
WV-OS-6	coarse	55
	med-coarse	60
	medium	60
	medium-fine	70
	fine	100
WV-McK-7a	coarse	20
	med-coarse	60
	medium	68

	medium-fine	82
	fine	87
WV-DS-9	coarse	40
	med-coarse	30
	medium	30
	medium-fine	90
	fine	95
WV-DM-10	coarse	25
	med-coarse	30
	medium	45
	medium-fine	65
	fine	85
WV-DS-11	coarse	30
	med-coarse	30
	medium	40
	medium-fine	80
	fine	85
MD-WC-12	coarse	35
	med-coarse	48
	medium	40
	medium-fine	65
	fine	70
MD-WC-13	coarse	40
	med-coarse	50
	medium	65

	medium-fine	80
	fine	90
MD-BF-14	coarse	20
	med-coarse	17
	medium	38
	medium-fine	65
	fine	90
MD-McK-16	coarse	30
	med-coarse	32
	medium	35
	medium-fine	55
	fine	80
PA-S-18	coarse	40
	med-coarse	55
	medium	72
	medium-fine	88
	fine	95
PA-DS-19	coarse	40
	med-coarse	60
	medium	70
	medium-fine	80
	fine	95
PA-BF-22	coarse	95
	med-coarse	60
	medium	65

	medium-fine	77
	fine	95
PA-DS-24	coarse	40
	med-coarse	30
	medium	50
	medium-fine	65
	fine	75
PA-WC-25	coarse	30
	med-coarse	50
	medium	50
	medium-fine	60
	fine	70
PA-RS-26	coarse	50
	med-coarse	65
	medium	80
	medium-fine	85
	fine	95
PA-F-28	coarse	55
	med-coarse	60
	medium	65
	medium-fine	70
	fine	80
PA-RSBE-31	coarse	48
	med-coarse	65
	medium	70

	medium-fine	85
	fine	88
PA-JF-32	coarse	70
	med-coarse	70
	medium	65
	medium-fine	88
	fine	95
PA-RH-33	coarse	50
	med-coarse	40
	medium	50
	medium-fine	87
	fine	92
PA-RS-35	coarse	45
	med-coarse	70
	medium	75
	medium-fine	80
	fine	85
PA-BF-36	coarse	10
	med-coarse	10
	medium	70
	medium-fine	80
	fine	80
PA-RH-37	coarse	45
	med-coarse	50
	medium	45

	medium-fine	100
	fine	100
PA-SS-40	coarse	30
	med-coarse	40
	medium	50
	medium-fine	95
	fine	100
PA-WC-42	coarse	40
	med-coarse	45
	medium	50
	medium-fine	92
	fine	100